Absorption spectrum of clusters of spheres from the general solution of Maxwell's equations. IV. Proximity, bulk, surface, and shadow effects (in binary clusters)

J. M. Gérardy
Institut Montefiore B28, Université de Liège, B-4000 Sart Tilman, Liège 1, Belgium

M. Ausloos
Institut de Physique B5, Université de Liège, B-4000 Sart Tilman, Liège 1, Belgium
(Received 9 June 1982)

From our solution of Maxwell's equations for aggregates of spherical particles, we answer questions such as: When is a particle isolated, or when can one *not* distinguish one small particle near or in contact with a larger one? In order to do so, the theory is limited to the dipolar approximation and applied to binary clusters of metallic particles; numerical results are presented specifically for sodium. The dielectric constant contains plasmon effects. A discussion of high-order polar effects is included.

I. INTRODUCTION

Much attention has been recently devoted to the prediction of the absorption modes and the shape of the absorption spectrum of clusters of particles. The necessity of studying clustering effects naturally arises since it is extremely difficult in experimental work to isolate a single particle of volume as low as 1000 Å^3, either because there is necessarily another particle nearby, or because instrumental techniques relying on "visual" observation are not sensitive enough to allow for the detection of a very small particle near a larger one.

Therefore several questions, which theoretical work can attempt to answer, are put forward. (1) What is the closest distance of approach for which a particle can be said to be isolated? (2) What are the "obvious" effects of a small particle next to a much larger one? (3) When are they important or negligible? (4) When can one observe or not a small particle next to a larger one? Following such an enumeration it appears that we are obviously concerned with a problem involving "small clusters," but similar questions can be asked in the context of studying larger clusters.

However, in such a case the cluster statistics is likely to be relevant and sufficient information is usually not available in the literature. In fact, attempts to describe the pair-correlation function for a powderlike system are rather rare. Usually very large clusters cannot be systematically reproduced, and any theory must rely on averaging procedures as done in the numerous works pertaining to the theory of the effective dielectric constant (EDC) of a random medium.[1] We have presented a simple "statistical" approach giving very reliable results elsewhere,[2] and following the same ideas as those presented in previous papers of this series.[3–7] However, it seems clear that information on the short-range order in a cluster is very important for describing an EDC. Therefore, further information on very small clusters has to be presented, not withstanding the more experimentally oriented questions listed here above.

Obviously the simplest cluster is the single particle. Mie,[8] Clanget,[9] Simanek,[10,11] and Ruppin[12] among others have studied independent particles. Effects of aggregation were nicely illuminated in the pioneer work of Clippe, Evrard, and Lucas[13] (CEL) based on a Hamiltonian (or dynamical matrix) description of interacting dipole fluctuation in spherical particles. Although limited to dipolar coupling, the CEL theory and subsequent work[14,15] could present some qualitative result in reasonable agreement with experimental optical spectra. Several discrepancies have been discussed by various authors,[13–18] and were somewhat resolved.

The most annoying features of CEL theory are likely the difficulty of including high-polar-order couplings (or charge-density fluctuations) which are very relevant when particles are close to each other and form dense clusters. The extreme case of very large random aggregates does not seem easily tractable due to the difficulty of introducing a clear statistical picture in the formalism, and of taking into account retardation effects. From an experimentalist view point, one can say that CEL theory could not reproduce the low-energy part of the optical spectrum and does not give back the bulk properties in the limit of large particles.

Our way to "extend" CEL theory was to solve Maxwell's equations as exactly as possible *to all po-*

lar orders.[3–7] In paper I of this series,[3] we presented the long-wavelength-limit solution and applied it to the ionic aggregate cases as those looked at by CEL. In paper II,[6] we presented the general theory in order to treat any arbitrary cluster geometry and any light incidence. Retardation effects as well as electric and magnetic interactions were included on the same footing. Metalliclike particles with given plasmon dispersion relations were studied. In paper III,[19] we have studied the case of inhomogeneous particles. In several cases, quadrupolar and octupolar interaction effects were looked at, e.g., for binary clusters,[3–7] linear chains,[3–7] tetrahedra,[7] and more complicated clusters.[4] We have proved that contributions from high-order polar interactions are important in not only modifying the position of absorption modes but also in introducing secondary structures.[3,4] Nevertheless, the amount of numerical calculation increases and becomes somewhat tedious when the size of the cluster grows or when the relative sizes of the particles are arbitrary. Furthermore, going beyond the dipolar approximation as we have done improves the agreement with experimental data, but does not give any better hint to the above questions than a simple calculation limited to the lowest-order approximation.

In fact, when applying our theory to the metallic particles in II, it was observed that the lowest-order approximation was already sufficient to distinguish various spectral regions.[6] The frequency region above the bulk-plasmon frequency ω_p consists in a large hump with very small ripples. A very different behavior is observed in the vicinity of the Fröhlich mode at $\omega_p/\sqrt{3}$. Therefore, the following results will serve to illustrate only the region below ω_p, and will only concern the binary-cluster case.

The theory is exactly that presented in paper II of this series,[6] and is summarized in Sec. II. However, we consider also the case in which the light propagation is parallel to the line joining the centers of the spheres. In Sec. III, one will see that in such a geometry "shadow effects" are observed.

It has appeared more pedagogical to group our results into two classes according to the size of one particle. Somewhat surprisingly, the results seem to be different indeed if one particle is very small (10 Å) or is of larger size (100 Å). We also treat the case of two equal-sized particles with increasing radii to explain such a surprising effect. Drawings (for a large number of cases) can illustrate the great variety of results "better than words" and they will represent in some sense "experimental results."

In Sec. IV we conclude this work by showing the various trends of absorption modes, and thus we answer the questions set in this introduction. We compare to other works. We also consider the effect of high-order polar interaction, but in the long-wavelength limit only (Appendix A).

II. TWO-SPHERE–CLUSTER THEORY

The theory which we follow is identical to that presented in Ref. 6. The solution of Maxwell's equation is established via the usual boundary conditions. If the fields are small enough such that the sum of the polarization and diffusion currents is proportional to the electric field, it is formally possible to solve Laplace's equation for a system of many spherical particles imbedded in a matrix. We refer the reader to paper II where the theory has been presented for the most general situation then. It is thus sufficient for our purpose to restrict at once the number of particles, and consider only two spheres of radius R_1 and R_2, separated by a distance $a \geq R_1 + R_2$. The particles are assumed to be made of the same metallic material and characterized by a plasmon frequency ω_p and a dielectric function ϵ (identical to that used by Ruppin[12] in the study of isolated particles). At the numerical stage, the parameters will be chosen to be those of sodium ($\omega_p = 8.65 \times 10^{15}$ Hz). The matrix is supposed to be vacuum. There are various ways of rewriting the general theory in the two-sphere–cluster case. In particular, because bispherical coordinates can be used[16,20,21] one can bypass the general transposition of spherical wave-vector functions from one reference frame to another.[3,6] Obviously, the number of resonant (ir active or not) modes does not depend on the formalism, but only varies with the number of multipoles considered to describe the charge-density fluctuations in each sphere.

As shown elsewhere (in the long-wavelength limit[3–5,7]) the high-order multipoles strongly influence the absorption modes. In principle, one obtains $l(l+3)$ resonant modes, where l is the exponent of 2 when the $2^l - 2^l -$ polar-interaction terms taken into account. However, depending on the light incidence several of these modes are inactive or degenerate. At arbitrary incidence, spectra become less easy to disentangle due to the finite amplitude of various competing modes. Furthermore, to keep high-order–interaction terms would greatly burden the calculation of the absorption spectrum without helping much in the discussion process. It is also observed that the "dipolar peak" has always the largest amplitude and governs the overall shape of the spectrum, while the peak position *trends* are not markedly influenced. Therefore in this section we have limited our study to $l=1$ and to the three simple geometries ($k_{\|}, E_{\perp\perp}, H_{\|}$) shown on Fig. 1: (1) When the wave vector k is parallel to the line joining the spheres centers (aligned on the z axis), (2) when the

wave vector is perpendicular to this line but the electric field $\vec{E}$ is parallel to z, and (3) when $\vec{k}$ and $\vec{E}$ are perpendicular to z, but the magnetic field $\vec{H}$ is parallel to z. It may immediately be said that geometries (1) and (3) give spectra which do not markedly differ from each other. Indeed in such cases, the influence of the electric field on the sphere polarization will be *almost* identical; the special differences are discussed below.

The dipolar electrical susceptibility of one of the spheres (say of radius R) in a matrix of dielectric constant ϵ_M is in general given by[6]

$$\Delta_q(R)=-\left[\frac{j_q(kR)}{h_q^{(1)}(kR)}\right]\frac{\epsilon_M[\hat{j}_q(k^TR)-f_q(k^LR)]-\epsilon^T[\hat{j}_q(kR)-f_q(k^LR)]}{\epsilon_M[\hat{j}_q(k^TR)-f_q(k^LR)]-\epsilon^T[\hat{h}_q^{(1)}(kR)-f_q(k^LR)]}\ , \tag{1}$$

where

$$\hat{g}(z)=g^{-1}(z)\frac{d}{dz}[zg(z)] \tag{2}$$

and

$$f_q(z)=q(q+1)j_q(z)\left[z\frac{d}{dz}j_q(z)\right]^{-1}\ . \tag{3}$$

Here k^L,k^T are, respectively, the longitudinal and transverse wave number inside the sphere, ϵ^T is the transverse dielectric constant inside the sphere, and $j_q(z)$ and $h_q^{(1)}(z)$ are the usual spherical Bessel functions.[22] The complex wave numbers k to be used are solving the dispersion relations

$$k^2c^2=\omega^2\epsilon^T(k,\omega)\mu(k,\omega)$$

for transverse waves and $\epsilon^L(k,\omega)=0$ for longitudinal waves in the appropriate medium; $\mu(k,\omega)$ is the magnetic permeability.

The general solution of Maxwell's equation for a random system of homogeneous spheres can be found in Ref. 6. The same notations are followed here. The incident wave ($\vec{k},\vec{E}_0,\vec{H}_0$) and the fields diffracted by the cluster embedded in the matrix (M) lead to a resulting field

$$\vec{E}_M=\vec{E}_0+E_0\sum_{i=1}^{2}\sum_{q,p}[c_{q,p}^M(i)\vec{m}_{qp3}(i)+d_{q,p}^M(i)\vec{n}_{qp3}(i)]\ , \tag{4}$$

$$\vec{H}_M=\vec{H}_0+H_0\sum_{i=1}^{2}\sum_{q,p}[d_{q,p}^M(i)\vec{m}_{qp3}(i)+c_{q,p}^M(i)\vec{n}_{qp3}(i)]\ , \tag{5}$$

where in the vicinity of one of the spheres (say j) the incident wave is

$$\vec{E}(j)=E_0\sum_{q,p}[a_{q,p}(j)\vec{m}_{qp1}(j)+b_{q,p}(j)\vec{n}_{qp1}(j)]\ , \tag{6a}$$

$$\vec{H}(j)=H_j\sum_{q,p}[b_{q,p}(j)\vec{m}_{qp1}(j)+a_{q,p}(j)\vec{n}_{qp1}(j)]\ . \tag{6b}$$

An extra term must be added to the right-hand side of Eq. (6a) in order to take into account the existence of longitudinal plasmons in the spheres; this additional term is

$$e_{q,p}(j)\vec{l}_{qp1}(j)\ . \tag{7}$$

The $\vec{m}_{qpi},\vec{n}_{qpi},\vec{l}_{qpi}$ functions are the usual spherical wave-vector functions (which can be expressed in terms of products of spherical Bessel functions with either Legendre polynomials or spherical harmonics[6]); the index $i=1$ or 3 indicates which Bessel function to use: j_q or $h_q^{(1)}$, respectively, depending on the required asymptotic behavior at zero or infinity.

The relation

$$H_j=ck_j^TE_0/[i\omega\mu(k_j^T,\omega)]$$

holds between the amplitudes in Eqs. (6) and (7). The usual boundary conditions,[23]

$$\vec{E}(j)\times\vec{l}_r=\vec{E}_M\times\vec{l}_r\ , \tag{8a}$$

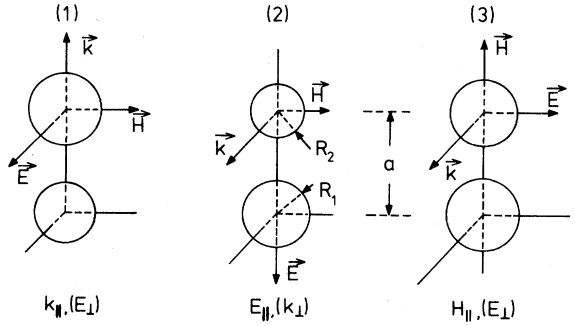

FIG. 1. Geometry of the incident electromagnetic plane wave ($\vec{k},\vec{E},\vec{H}$) with respect to the symmetry (z) axis of the binary cluster: (1) $k_{||}(E_\perp,H_\perp)$, (2) $E_{||}(k_\perp,H_\perp)$, and (3) $H_{||}(k_\perp,E_\perp)$.

$$\vec{H}(j)\times\vec{1}_r=\vec{H}_M\times\vec{1}_r\ , \tag{8b}$$

$$\vec{E}(j)\cdot\vec{1}_r=\vec{E}_M\cdot\vec{1}_r\ , \tag{8c}$$

hold on the surface of the sphere j of radius R_j. Through them, one can relate the coefficients inside the particle to that in the matrix. This can be done for both spheres, and through Jeffreys' theorem which relates spherical harmonics defined in different reference frames,[24] one obtains a system of linear equations for the unknown coefficients of interest (i.e., those outside the spheres)

$$\Delta_l^{-1}(j)d_{l,m}^M(j)-\sum_{i=1}^{2}{}'\sum_{q,p}[c_{q,p}^M(i)\mathscr{C}_{qplm}(i,j)+d_{q,p}^M(i)\mathscr{D}_{qplm}(i,j)]=b_{l,m}(j)\ , \tag{9}$$

$$\Gamma_l^{-1}(j)c_{l,m}^M(j)-\sum_{i=1}^{2}{}'\sum_{q,p}[c_{q,p}^M(i)\mathscr{D}_{qplm}(i,j)+d_{q,p}^M(i)\mathscr{C}_{qplm}(i,j)]=a_{l,m}(j)\ , \tag{10}$$

where the interaction terms $\mathscr{C}_{qplm}(i,j)$ and $\mathscr{D}_{qplm}(i,j)$ have a simple form[6] when $q=p=1$, and

$$\Gamma_q(R)=-\left[\frac{jq(kR)}{h_q^{(1)}(kR)}\right]\left[\frac{\mu\hat{j}_q(k_j^TR)-\mu_j\hat{j}_q(kR)}{\mu\hat{j}_q(k_j^TR)-\mu_j\hat{h}_q^{(1)}(kr)}\right] \tag{11}$$

is the 2^q polar-order magnetic susceptibility of the sphere. In those equations, the summations [usually over $q=(1,\infty)$ and $p=(-q,+q)$] will thus be truncated at $q=1$.

The system of linear Eqs. (9) and (10) can be written in matrix form, and reads $\mathscr{A}^{(|m|)}\vec{d}=\vec{b}$, with

$$\mathscr{A}^{(|m|)}=\begin{bmatrix} 1 & -\Delta_1^{(1)}V_{11}^{(|m|)}(ka) & 0 & \mp W_{11}^{(|m|)}(ka)\Delta_1^{(1)} \\ -\Delta_1^{(2)}V_{11}^{(|m|)}(ka) & 1 & \pm W_{11}^{(|m|)}(ka)\Delta_1^{(2)} & 0 \\ 0 & \mp\Gamma_1(1)W_{11}^{(|m|)}(ka) & 1 & -V_{11}^{(|m|)}(ka)\Gamma_1^{(1)} \\ \pm\Gamma_1^{(2)}W_{11}^{(|m|)}(ka) & 0 & -V_{11}^{(|m|)}(ka)\Gamma_1^{(2)} & 1 \end{bmatrix}, \tag{12}$$

where the upper (lower) sign is used for $m=+1$ (-1), $\vec{d}=(d_{1,|m|}^{(1)},d_{1,|m|}^{(2)},c_{1,|m|}^{(1)},c_{1,|m|}^{(2)})$, and $\vec{b}=(b_{1,|m|},b_{1,|m|}e^{i\vec{k}\cdot\vec{a}},a_{1,|m|},a_{1,|m|}e^{i\vec{k}\cdot\vec{a}})$, while

$$V_{11}^{(|m|)}(x)=B_{11}^{(|m|)}(x)\sum_{j=0}^{3-|m|}i^{j-|m|}x^{-j}v_{11}^{(|m|)}(j)\ , \tag{13}$$

$$W_{11}^{(|m|)}(x)=-B_{11}^{(|m|)}(x)\sum_{j=0}^{2-|m|}i^{j-|m|}x^{-j}w_{11}^{(|m|)}(j)\ , \tag{14}$$

with

$$B_{11}^{(|m|)}(x)=\frac{3}{2}\frac{e^{ix}}{x^{|m|}}\frac{(|m|!)^2(1-|m|)!}{(1+|m|)!}\ . \tag{15}$$

The $v_{11}^{(|m|)}(j)$ and $w_{11}^{(|m|)}(j)$ coefficients are given in Table I.

The inhomogeneous terms (right-hand side) of Eqs. (9) and (10) are easily obtained from the general theory but are concisely rewritten here in the dipolar order case, i.e.,

$$a_{1,m}=-(3\pi)^{1/2}[e^{-i\gamma}O(1,1,m-\alpha)+e^{i\gamma}O(1,-1,m,-\alpha)]e^{ik_za}\ , \tag{16a}$$

TABLE I. Value of the coefficients $v_{11}^m(j)$ and $w_{11}^m(j)$ necessary to calculate the elements $V_{11}^{(|m|)}(a)$ and $W_{11}^{(|m|)}(a)$ in Eqs. (13) and (14) for the various mode polarizations ($m=0,\pm1$).

	$v_{11}^m(j)$				
m \ j	0	1	2	3	4
0	0	0	2	2	0
±1	2	2	2	0	0

	$w_{11}^{(m)}(j)$		
m \ j	0	1	2
0	0	0	0
±1	2	2	0

$$b_{1,m}=-(3\pi)^{1/2}[e^{-i\gamma}O(1,1,m,-\alpha) - e^{i\gamma}O(1,-1,m,-\alpha)]e^{ik_z a}, \tag{16b}$$

where γ is the angle between the $\vec{H}_0$ vector and the intersection of the (x,y) plane with the $(\vec{E}_0,\vec{H}_0)$ plane as shown on Fig. 2, while α is the angle between the z axis, i.e., the line joining the sphere centers, and the $\vec{k}$ vector. The $O(n,m,l,\alpha)$ coefficients are those which we have called the Jeffreys' coefficients,[6]

$$O(n,m,l,\alpha)=(-)^{n+l}[(n+m)!(n-m)!(n+l)!(n-l)!]^{1/2}\sum_{r=f}^{g}\frac{(-)^r[\cos(\tfrac{1}{2}\alpha)]^{2r+m+l}[\sin(\tfrac{1}{2}\alpha)]^{2(n-r)-m-l}}{r!(n-m-r)!(n-l-r)!(m+l+r)!}. \tag{17}$$

The integer r spans the interval bounded by $f=\max(0,-m-l)$ and $g=\min(n-l,n-m)$. Since one of the spheres (say, 1) is placed at the origin and the other is located at a coordinate a on the positive (negative) z axis, the above coefficients take simple values, since then $\alpha=0(\pi)$, while $\gamma=0,\pm\pi/2,\pm 3\pi/2$, depending on the experimental geometries considered (Fig. 1). One easily finds that only the $m=0$ term survives since $a_{1,\pm1}=b_{1,\pm1}=0$ in such cases. The resonant mode frequencies ω_μ are thus simply obtained by searching for the zeros of $\det\mathscr{A}=0$.

Let us stress here the importance of keeping the coupling between magnetic and electric interactions, in particular in order to describe the so-called shadow effect (Sec. V) and because we have not taken a long-wavelength limit. Indeed, if one would neglect $W_{11}^{(|m|)}(x)$, the matrix equation would be separable into purely magnetic and electric parts. The latter would only give two resonant modes[13] when $R_1=R_2$, i.e., if $\Delta_1(1)=\Delta_1(2)$, as in CEL.

III. NUMERICAL RESULTS

One can now display the various modes as a function of the size of the particles. In order to answer the questions listed in Sec. I, it seems better to display the absorption spectrum and observe its evolution as it would be done experimentally. The maxima in the spectrum will be supposed to occur at the resonant-mode frequencies. The maxima are usually very sharp. Their position on a ω/ω_p scale is accurate within a $\pm 1.25\%$ error due to the finite mesh of our integration process.

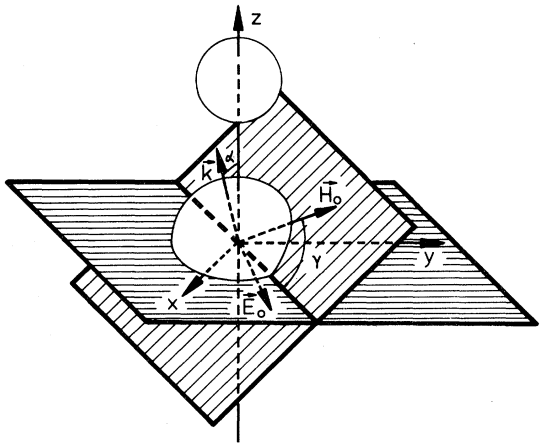

FIG. 2. Arbitrary wave-incidence geometry on a binary cluster, thereby defining the polarization angle γ [Eq. (16)]. (See also Appendix B.)

The absorption coefficient which we calculate is in fact the reduced "extinction cross section,"[6]

$$\sigma_e=-\xi^{-2}\sum_{m=-1}^{+1}\mathrm{Re}(b_{1,m}^{*(1)}d_{1,m}^{M(1)}+a_{1,m}^{*(1)}c_{1,m}^{(1)} +a_{1,m}^{*(2)}c_{1,m}^{M(2)}+b_{1,m}^{*(2)}d_{1,m}^{M(2)}), \tag{18}$$

with $\xi^2=\pi k^2(R_1^2+R_2^2)$.

The results are separated into two groups according to the size of one of the particles, e.g., $R_1=10$ Å or $R_1=100$ Å. Three different light polarizations have been studied (Fig. 1). The spectra corresponding to noninteracting (or single) particles[16] are also given. The logarithm of the extinction cross section is plotted as a function of the reduced frequency $\bar{\omega}=\omega/\omega_p$. As previously justified, only the portion between 0.2 and 1.0 is shown. Let us recall that the resonant Fröhlich mode in the long-wavelength limit for such sodium spheres occurs at $\omega_s=\omega_p/\sqrt{3}=20.654$ eV and is (then) radius independent.

We could have chosen to display particular cases, but we feel that the evolution of the spectra would not be so clearly demonstrated, although by presenting several small drawings we realize that we demand a somewhat greater visual effort, but also limit the length of this report.

The noninteracting- (NI-) sphere case is the superposition of two single-particle-absorption spectra as obtained from Ruppin's theory. Owing to the k dependence of the dielectric function their absorption maximum occurs at different frequencies. The strength of the maximum also depends on the sphere dipole moment and thus differs for both spheres if they have unequal volume. Such differences might

appear minute on several spectra and are sometimes only seen as shoulders. Finally, the NI-sphere absorption spectra are easily distinguishable from the interacting-sphere spectra because the former are drawn as dotted lines near their absorption maxima. Notice that the vertical scale may differ from figure to figure in order to insure some drawing clarity, but in fact to respect relative sizes.

A. $R_1 = 10$ Å, $R_2 = (1, \ldots, 230$ Å), and $a = R_1 + R_2$

In Figs. 3 and 4, we show spectra for very-small- to medium-size spheres (R_2) in contact with a rather small one (R_1). When the spheres have the same 10-Å radius, the spectrum is very simple: a single peak seems to be present only (see below, however). When radii differ (e.g., $R_1 = 10$ Å, $R_2 = 20$ Å) the spectrum splits into two peaks on both sides of ω_s; the $E_{||}$ peaks are further apart than the $E_{\perp}$ peaks. This would lead to a more complicated peak structure at arbitrary incidence but only when R_2/R_1 is less than 5. When one of the spheres grows such that $R_2/R_1 \simeq 8$ as on Fig. 3, the light polarization becomes irrelevant, and the spectrum has a simple two-peak structure of quite different amplitudes. The main peak is approximately located at ω_s. When R_2/R_1 is about equal to 23 (undisplayed case), the smaller peak at higher frequency appears as a *very small* shoulder and would likely be undistinguishable from the background. On Fig. 4, we show the spectra for a small-sized sphere ($R_1 = 10$ Å) in contact with a very small one. At first except for the main-peak position, the spectra looks similar to that of Fig. 3. However, when the ratio R_2/R_1 becomes smaller than 0.5 the peak structure becomes light incidence independent. The upper frequency peak "rapidly" moves toward higher frequency with decreasing R_2/R_1. Furthermore, the latter peak in the $E_{||}$ geometry disappears when $R_2/R_1 \simeq 0.4$, while the lower peak becomes polarization independent below such a value. Its position saturates at a reduced frequency ω_M/ω_p equal to that characterizing the surface mode of the $R_1 = 10$ Å sphere when the latter is in contact with a very large sphere.

B. $R_1 = 100$ Å, $R_2 = (1, \ldots, 300$ Å), and $a = R_1 + R_2$

At first somewhat surprisingly we found the spectrum of two equal-sized spheres of radius 100 Å to be rather different than that for the $R_1 = R_2 = 10$ Å spheres. Figure 5 shows the drastic effect of the light polarization in the case $R_1 = R_2 = 100$ Å. In the $E_{||}$ incidence, one observes a single peak at low energy, while in the $(E_{\perp}, H_{||})$ configuration the absorption peak occurs above ω_s. However, when the incident wave vector is parallel to the center to center axis and both E and H are perpendicular to this axis (i.e., $k_{||}$ geometry), an extra peak of lower amplitude but very distinguishable occurs below ω_s. Owing to this type of "experimental geometry" we called such a behavior the shadow effect.

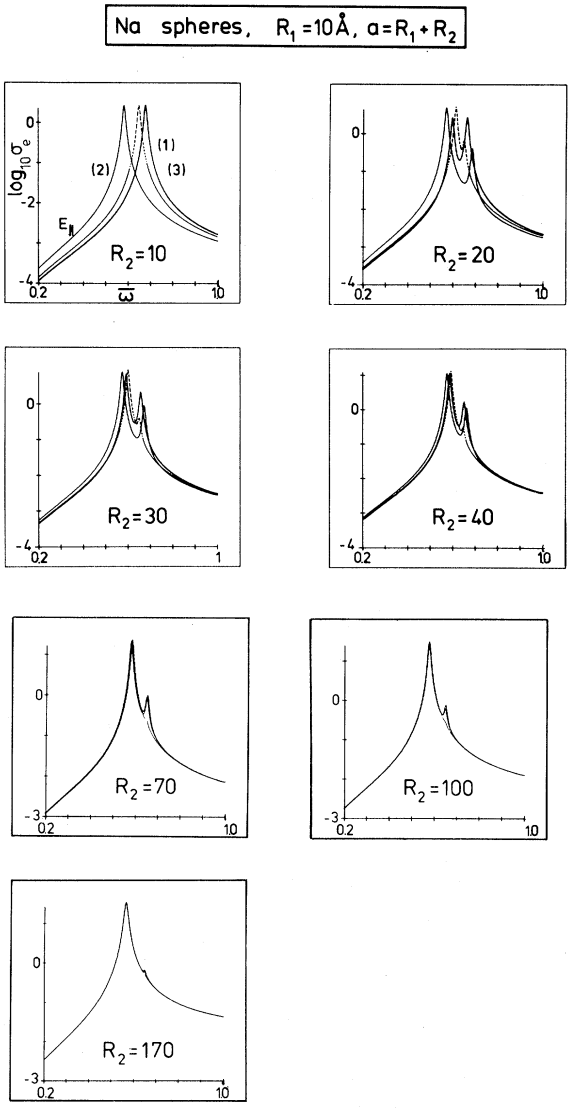

FIG. 3. Logarithm of the dipolar extinction cross section σ_e for two touching and interacting sodium spheres (of magnetic permeability $\mu = 1$) in a vacuum matrix in variously polarized ($k_{||}$, $E_{||}$, or $H_{||}$) plane waves. Radius of one sphere is constant, $R_1 = 10$ Å, and $R_1 \leq R_2 \leq 230$ Å as indicated. Noninteracting-sphere case is shown by dashed lines in the vicinity of the absorption maxima; $\bar{\omega} = \omega/\omega_p$.

When the radius of one of the spheres grows, the single-peak structure for $E_{||}$ and $H_{||}$ becomes a two-peak structure as in the previous ($R_1 = 10$ Å) case, and the shadow effect in some sense disappears.

When $R_2 \simeq 5R_1$ again the main peak is close to

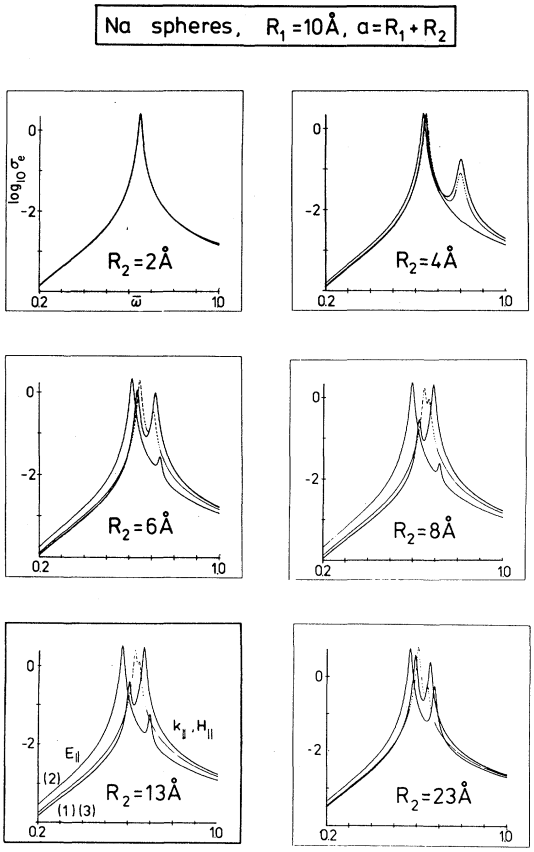

FIG. 4. Same as Fig. 3, but for $R_1=10$ Å and $R_2 \leq 23$ Å as indicated.

the Fröhlich mode and the light polarization becomes rather irrelevant leading to a double-peak structure of not too different magnitude on a logarithmic scale. When R_2 increases further some structure still occurs at higher frequency where the experimental geometry has some moderate influence but the main peak is close to that of an isolated sphere. Such a small structure remains visible (but is not shown) up to $R_2/R_1=23$ on our expanded scales.

Spectra for a medium-size sphere ($R_1=100$ Å) in contact with a small- or a medium-size sphere are shown in Fig. 6. The scattering-geometry—dependent peak structure reduces to a geometry-independent structure below $\rho=R_2/R_1$ about equal to 0.1. The low- and high-frequency peaks, respectively, stabilize at ω_s/ω_p and ω_M/ω_p.

C. $R_1=R_2$, $a=R_1+R_2$, and $R_1=(15,\ldots,1000$ Å)

Because of the previously noted shadow effect when $R_1=R_2$ it seems interesting to observe the behavior of the binary *equal-sized*—sphere cluster in greater detail as a function of both sphere radius. In

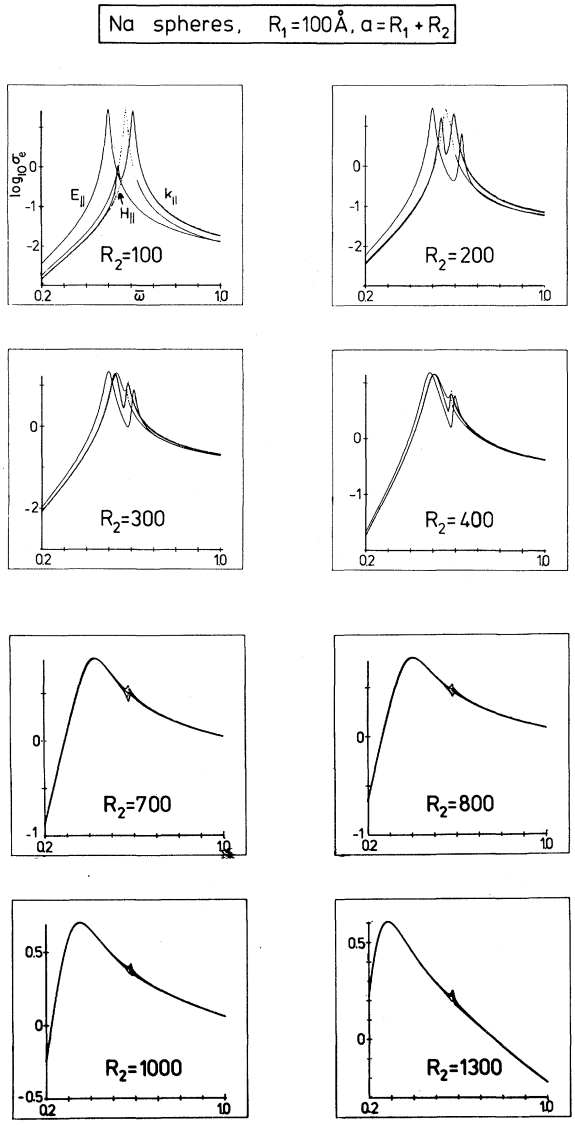

FIG. 5. Logarithm of the dipolar extinction cross section σ_e for two touching and interacting sodium spheres (with magnetic permeability $\mu=1$) in a vacuum matrix in variously polarized plane waves ($E_\parallel$, $k_\parallel$, or $H_\parallel$). Radius of one particle is constant, $R_1=100$ Å, while the other R_2 is such that $R_1 \leq R_2 \leq 1300$ Å. Axes and lines as on Fig. 2.

Fig. 7 we show how the shadow effect develops. In the case of rather small spheres ($R_1=R_2=10$ Å), we recall that no such effect was seen (Fig. 3). However, when $R_1=R_2=15$ Å, an acute observer can notice a shoulder developing on the $k_\parallel$ curve slightly below the "noninteracting-sphere peak" (Fig. 7), becoming more pronounced as soon as $R_1=R_2=30$ Å and leading to a three-peak equal-height structure for $R_1=R_2=200$ Å.

To let the spheres grow further is also of interest

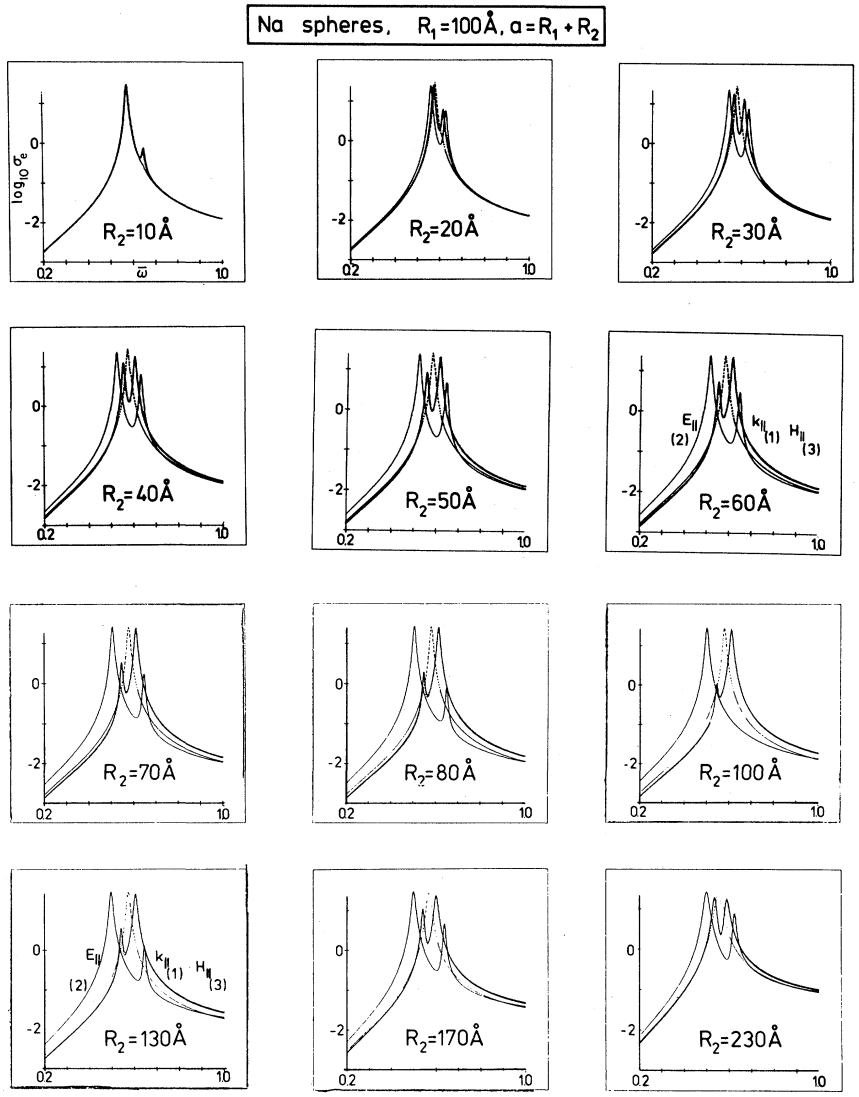

FIG. 6. Same as Fig 5, but for $0 \leq R_2 \leq 230$ Å as indicated.

in order to observe the trends of the resonant modes, e.g., toward characteristic bulk frequencies. We have calculated, but not shown, the spectra for large spheres (as large as 5000 Å); but for $R_1 = R_2 \geq 1000$ Å, the spectrum reduces to a large bump plus a small but distinguishable structure at high ω.

D. Single-particle limit (R_1 or $R_2 \to 0$)

It seems of interest to consider the modes both near $R_1 \simeq 0$ or $R_1 \gg R_2$. In order to obtain precisely quantities like ω_M / ω_p, we thus examine the special case of a "point dipole" ($R_1 \to 0$) in contact with a sphere of radius R_2, and observe the position variation of the pure surface mode. In Eq. (12) we let $a = R_2$, $\Delta_1(R_1 \to 0)$ and $\Gamma_1(R_1 \to 0)$; this is equivalent to making the long-wavelength limit approximation for *one* of the spheres only. The resonant-mode position is shown on Fig. 8 when R_2 grows from 1 to 1000 Å. Thus, we show the evolution of the single- (isolated-) particle surface mode as a function of the particle radius due to the k dependence of the dielectric constant.

E. Arbitrary incidence

When the electromagnetic wave incident upon the binary cluster does not have any of the $\vec{k}$, $\vec{E}$, or $\vec{H}$ vectors parallel to the z axis, the absorption spectrum becomes a linear superposition of the above spectra. The weighting factors for the amplitude depend on the (square of the) cosine between $\vec{E}$ and z,

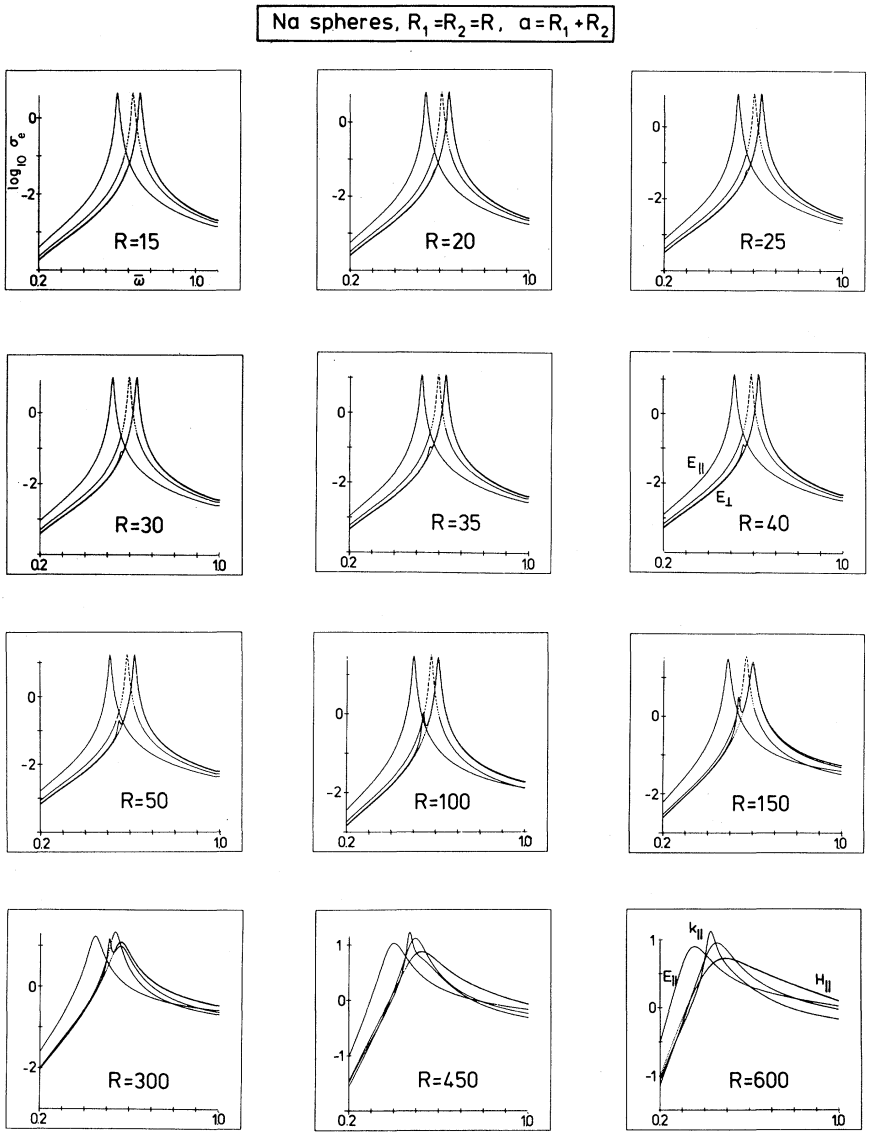

FIG. 7. Logarithm of the dipolar extinction cross section of two interacting *equal-sized* sodium spheres (with magnetic permeability $\mu=1$) in contact. Electromagnetic wave polarization is indicated ($k_{||}$, $E_{||}$, or $H_{||}$). Sphere radii vary between 15 and 600 Å as indicated.

of course, but the positions of the absorption peaks remain unchanged. In Fig. 9, we have for the sake of illustration singled our four characteristic cases previously examined under symmetrical light incidence geometry: (a) $R_1=10$ Å and $R_2=20$ Å (Fig. 3), (b) $R_1=100$ Å and $R_2=200$ Å (Fig. 5), (c) $R_1=R_2=300$ Å, and (d) $R_1=R_2=150$ Å (both treated in Fig. 7). The "symmetrical-geometry cases" (1)—(3) as defined in Fig. (2) have been reproduced anew, but all have been drawn as dotted lines in order to make more apparent the effect of an oblique $\vec{k}$ vector with respect to the cluster symmetry axis. Two angles have been considered and are called geometries (4) and (5), respectively, i.e., $\gamma=\pi/4$ and $\gamma=2\pi/3$. In both cases, α (as defined in Sec. II) is equal to $\pi/4$. It is noticable from observation of the lowest-frequency absorption peak that the amplitude decreases when γ changes in such a way that the $\vec{E}$-vector component along the z axis decreases. The amplitude of the higher-frequency peaks are modified accordingly.

This observation holds true whether the spheres have equal sizes or not. In the former case, even it is worth noticing that the spectrum is composed of a

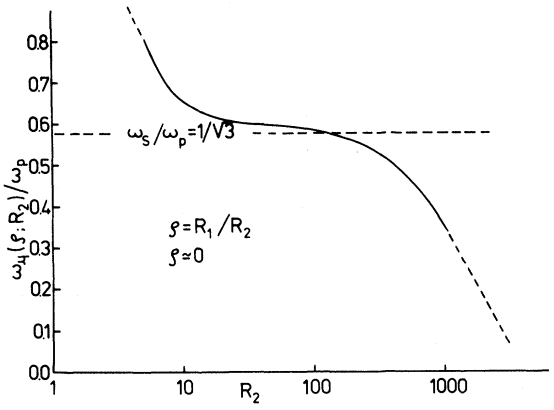

FIG. 8. Variation of the single-particle resonance mode as a function of the finite-size particle radius R_2 for a k-dependent Lindhard dielectric constant.

variety of peaks, in particular for clusters made of rather large-size particles. A four-peak structure is observed [Fig. 9(c)] for "arbitrary" incidence in contrast to a single-peak [geometries (1) and (2)] or a two-peak structure [geometry (3)]. In the medium-size case, $R_1=R_2=150$ Å, a sharp two-peak structure is observed with a very noticeable shoulder due to a remnant shadow effect [Fig. 9(d)].

For different-size particles [as on Figs. 9(a)—9(b)], the multiple-peak structure collapses into a three- then a two-peak structure whatever the geometry when the radius ratio (R_2/R_1) decreases (Fig. 4), irrespectively of the absolute size of the particles.

Therefore, in a powder made of binary clusters of various-size spheres, the absorption spectrum would also be a combination of such peaks and would thus consist of a rather broad absorption band with

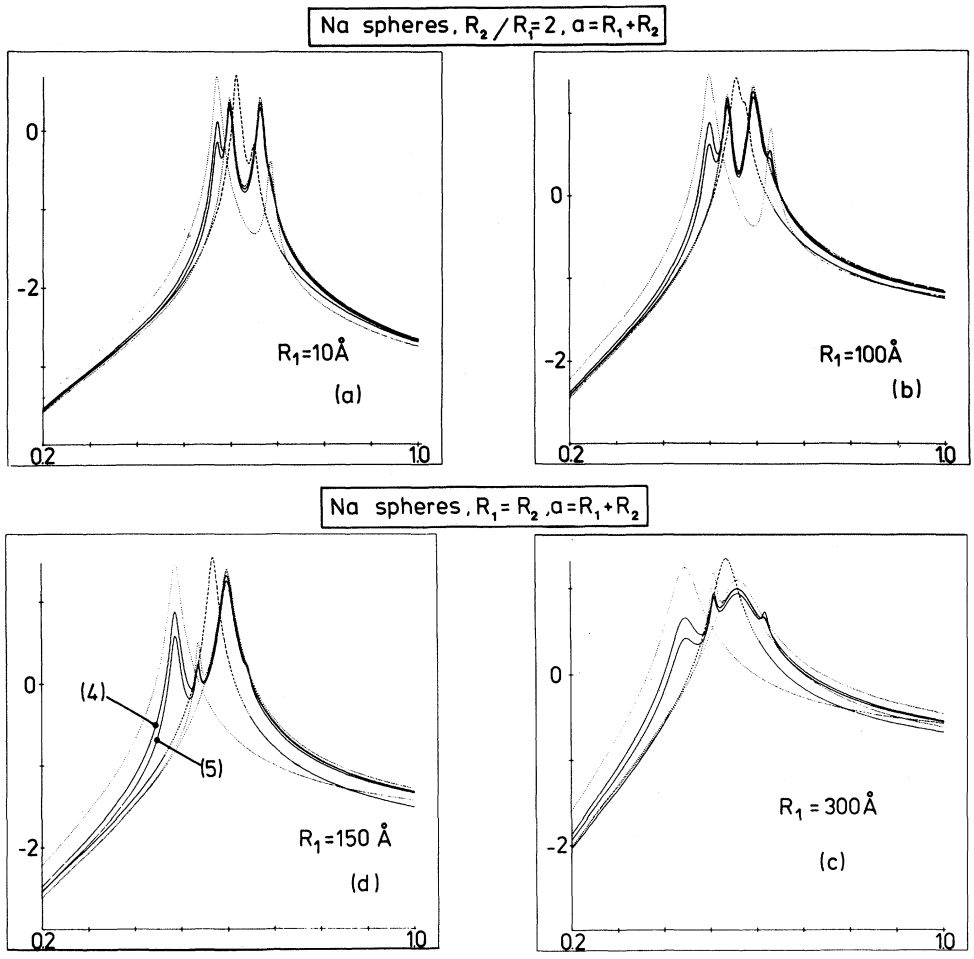

FIG. 9. Logarithm of the dipolar extinction cross section σ_e as a function of the reduced frequency $\bar{\omega}=\omega/\omega_p$ for binary clusters of sodium spheres *in contact* and placed in a vacuum matrix: (a) $R_1=10$ Å, $R_2=20$ Å, (b) $R_1=100$ Å, $R_2=200$ Å, (c) $R_1=R_2=300$ Å, and (d) $R_1=R_2=150$ Å. Variously polarized incident waves are considered. Dotted lines (in the vicinity of absorption maxima) correspond to the three symmetrical geometries (1), (2), and (3) of Figs. 2—7; dashed line corresponds to the noninteracting-sphere cases. Continuous lines are for "arbitrary incidences," i.e., the angles γ and α (as defined in Sec. II) take the values (4) $\gamma=\alpha=\pi/4$ and (5) $\gamma=2\pi/3,\alpha=\pi/4$.

nevertheless some smooth structure. If the density of clusters is not too large, such that cluster-cluster interactions can be neglected, and if the size distribution is not too broad (as usually expected in laboratory situations) the above observations could be usefully taken in order to analyze spectra and derive the distribution of cluster orientations in a matrix. It would be sufficient to shine some light at various incidences indeed. If one of these conditions is not fulfilled, some spectrum analysis would rather have to follow from applications of the theory sketched in Ref. 2.

IV. LONG-WAVELENGTH LIMIT

In the long-wavelength limit ($k \to 0$), the plasmon dispersion relation does not influence much the dielectric constant of the particles. In fact $\epsilon^T(,\omega)$ and $\epsilon^L(k,\omega)$ reduce to the Drude dielectric constant. When only dipolar terms are included as here, our theory reduces to that of CEL,[13] hence leading to the usual peak positions for the Clippe modes. The spectra have been calculated for all cases considered above, but are not displayed. Nevertheless the mode positions are somewhat different from those found in the general theory as discussed in Sec. V, where the numerical comparison will be found.

Let us warn the reader about a slight change in normalization between the usual dipolar electrical resistivity in the long-wavelength limit, i.e.,

$$\Delta_1^{(0)}(R)=(\epsilon-\epsilon_M)R^3(\epsilon+2\epsilon_M)^{-1}\ , \tag{19a}$$

and the $k \to 0$ value of the general definition (1), which is here,

$$\lim_{k\to 0}\Delta_1(R)=(2i/3)(\epsilon-\epsilon_M)R^3(\epsilon+2\epsilon_M)^{-1}\ , \tag{19b}$$

where we have also taken the plasmonless limit, i.e., $f_q(k_j^L R)=0$ in geometry (1).

In the long-wavelength limit, the system of linear equations for the unknown field coefficients is simply written

$$(\Delta_n^{(0)}(i))^{-1}d_{n,m}(i)+\sum_{qpj} d_{q,p}(j)h_{qpnm}(i,j)e^{ik_z a} = -b_{n,m}(i)e^{i\vec{k}\cdot\vec{r}_i}\ , \tag{20}$$

where

$$h_{qpnm}^{(i,j)}=(-)^n\frac{(q+n)!}{a^{q+n+1}}\left[\frac{2q+1}{2n+1}\right]^{1/2}\delta_{p,m}\sum_{l=-d}^{+\phi}(-)^l\frac{O(q,p,l,\alpha)O(n,m,l,\alpha)}{[(n+l)!(n-l)!(q+l)!(q-l)!]^{1/2}}\ , \tag{21}$$

and the $O(n,m,l,\alpha)$ coefficients have been defined in (17). Their values in the dipolar case are given in Table II for an arbitrary angle of incidence (α) between $\vec{k}$ and the z axis, and $d=\min(q,n)$.

In this limiting case, the $kR \ll 1$ assumption leads to an enormous simplification indeed since electric and magnetic multipole terms uncouple, in contrast to the general case worked out in Sec. II. In the latter case it was necessary to display the magnetic multipole terms in, e.g., Eq. (12). In the long-wavelength limit, such terms are negligible since they are, in general, a factor $(kR)^2$ smaller than their corresponding electrical equivalent. Notice, however, that in the long-wavelength limit, high-order electric multipoles are produced by the mere effect of multiparticle interactions in particular at small-sphere separations. Such effects are further analyzed in Appendix A.

V. DISCUSSION

The question on the closest distance of approach for which a particle can be said to be isolated was already answered in Ref. 6. For *small* metal particles in vacuum with an equal radius of the order of 15 Å, two particles can be said to be isolated when their center separation a is about $5R$. For unequal-sized *small* spheres their mutual influence was found to be rather negligible when their separation was also about 5 times the larger radius. Notice that if *both* spheres are rather *large* (e.g., $R_1=35$–500 Å), the small sphere spectrum is totally washed out by that of the large one at a much shorter distance, e.g., $a \simeq 2R_2$ when $R_2/R_1=10$ (Fig. 10). When the spheres are very close to each other, their mutual influence becomes more important, even in the dipolar approximation. In this case, as soon as the particles have a radius equal to 15 Å, the Fröhlich mode of the upper frequency resonance splits into a double structure in the $k_{||}$ geometry (Figs. 3 and 7).

On the other hand, we have seen in Figs. 3 and 5

TABLE II. Jeffreys' coefficients limited to the dipolar order. $C=\cos\alpha/2$, $S=\sin\alpha/2$.

l \ m	-1	0	$+1$
-1	C^2	$-\sqrt{2}CS$	S^2
0	$\sqrt{2}CS$	C^2-S^2	$-\sqrt{2}CS$
$+1$	S^2	$\sqrt{2}CS$	C^2

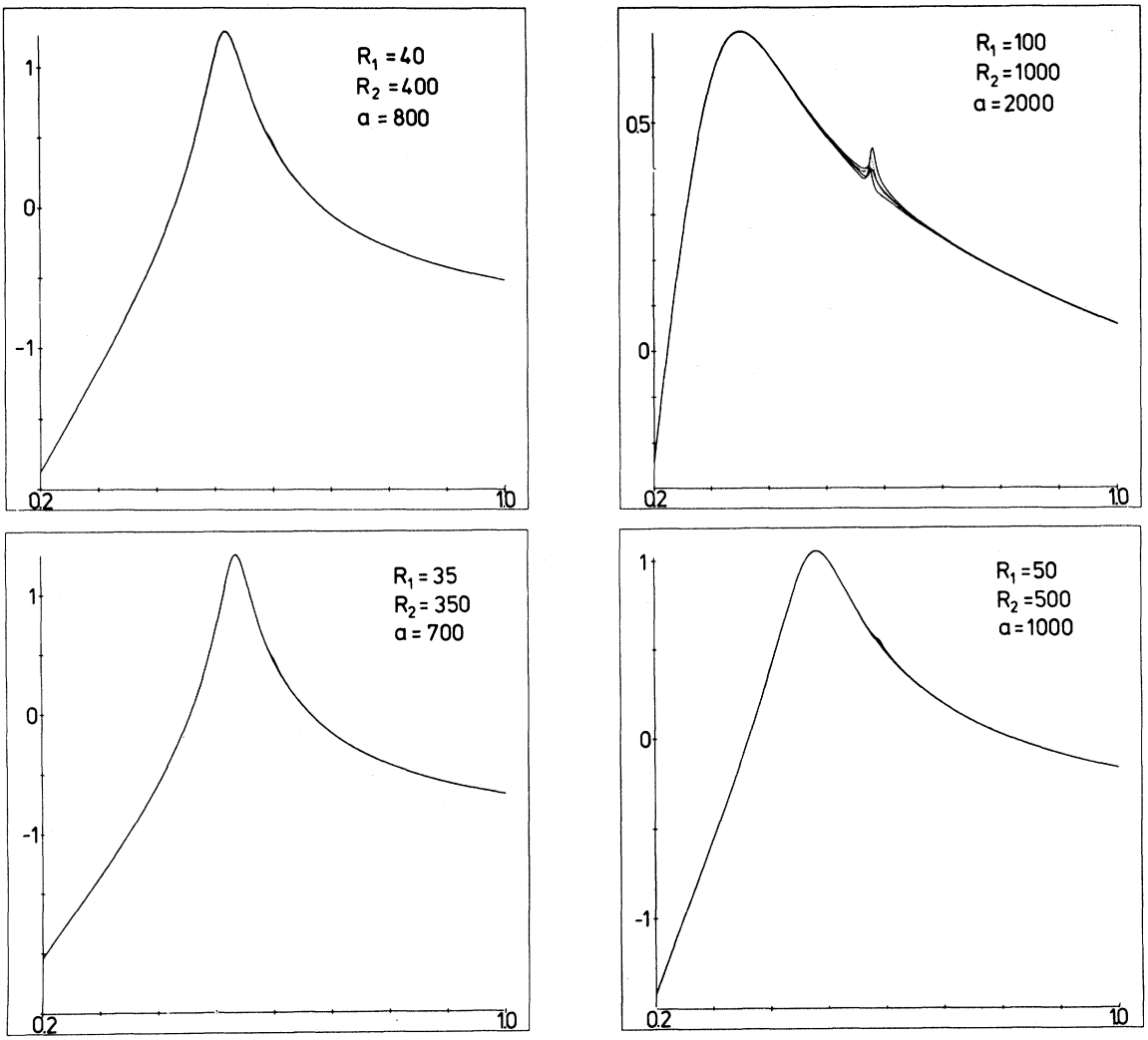

FIG. 10. Logarithm of the dipolar extinction cross section for two unequal-sized *nontouching* but interacting sodium spheres (with magnetic permeability $\mu=1$) for variously polarized incident electromagnetic waves. The distance between the centers of the particles is $a=2R_2$, where R_2 is the radius of the larger particle as indicated. Smaller particle has a radius $R_1=R_2/10$.

that the critical size for which the larger particle masks the smaller one is reached when $R_1/R_2=23$, *when both spheres are in contact.*

Besides this experimentally useful information, very interesting other features can be inferred from the spectra evolution, in particular concerning the mode positions. Furthermore, this allows us some comparison to other pertinent theoretical results.

The second and third questions asked in the Introduction concern the effect of a neighboring particle on the absorption peaks. Let us recall the seemingly contradictory experimental results of Smithard and co-workers[25,26] on sodium particles on one hand, and of Genzel, Martin, and Kreibig,[27] on the other hand, on silver particles. The first group has found a shift of the resonance toward longer wavelengths (or smaller frequencies), in particular for particles with a radius greater than 40 Å, in agreement with model calculations based on a classical mean-free-path (or dielectric-constant) approach. In such a theory, the absorption hardly shifts for smaller-size particles, as was also found by Smithard and Tran.[25] However, a shift of the "optical plasma resonance" toward lower wavelengths (higher frequencies) was observed in Ref. 27, when the particle size is decreasing as predicted by quantum-mechanical calculations (see Ref. 28 for an excellent and very recent review). As recalled in the latter reference, several attempts have been made in order to reconcile these contradictory results. One of them was the in-

clusion of plasmon contributions in the dielectric constant. It revealed secondary structures above ω_p (thus at lower wavelengths) which could not be seen on the data of Ref. 27, while the main resonance was systematically shifted toward lower frequencies with respect to the classical Mie prediction apparently whatever the particle size.

From our displayed results on (very) small particles we propose that a plausible explanation of the discrepancy lies in the fact that the absorption spectrum is due to a combination of resonances strongly depending on the proximity of neighboring particles, and the maximum-absorption position thus depends on the particle distribution in the sample. (In other words, a particle-distribution function might be necessary before a definite conclusion is made). However, we will observe next that the main absorption peak shifts toward higher frequencies when the particle size *decreases,* even when proximity effects are taken into account[29] (see also Fig. 8).

First consider again the case of a $R_1=10$ Å particle next to another of radius R_2 growing from 0 to "infinity." For an arbitrary experimental light incidence, two (small-amplitude) modes originate from ω_p and tend toward the value $\omega_M/\omega_p=0.6475$ which they reach at about $\rho\simeq 13$. The other two (degenerate) surface modes originating from this ω_M/ω_p value at $\rho=0$ fall steadily (Fig. 11) toward $\omega_{k_{\|}}^{(1)}\cong\omega_{H_{\|}}^{(1)}=0.6124\omega_p$ and $\omega_{E_{\|}}^{(1)}=0.583\omega_p$ at $\rho=1$. The former modes (dashed line) have some smooth decreasing behavior, but the latter (solid line) goes through a minimum at $\rho=2$ below the ω_s/ω_p value, rises above the Fröhlich-mode value between $\rho\simeq 5$ and 10, and finally merges into the noninteracting-mode (dotted) line like the $E_{\perp}$ modes. It seems interesting to notice that this isolated-particle surface mode is radius dependent (due to the k dependence of the dielectric constant), and is continuously but slowly decreasing. On the same figure, we have shown the variation (CA line) of the resonant-mode position of a recent extension of the CEL theory by Clippe and Ausloos (CA).[15] Such a work takes into account the dipole-dipole coupling between spheres of unequal radii, but in the long-wavelength limit, and thus leads to a symmetrical relation in ρ and ρ^{-1}, i.e.,

$$\omega_\mu^2(\rho)/\omega_p^2=[\omega_\mu^2(1)/\omega_p^2][1-f(\rho)]+f(\rho)/3\ , \tag{22}$$

where

$$f(\rho)=1-8\rho^{3/2}(1+\rho)^{-3}=f(1/\rho)\ . \tag{23}$$

In order to draw the CA lines, we have used the Drude k-independent dielectric constant $\epsilon(\omega)=1-\omega_p^2/\omega^2$. In such a case, one predicts four types of modes, two of them correspond to the Clippe modes (at $\rho=1$ thus), i.e., a high-amplitude low-frequency $m=0$ mode, and a doubly degenerate $m=\pm 1$ mode of smaller amplitude at high ω. The former goes through a minimum when $\epsilon+3=0$ at $\omega_\mu/\omega_p=0.5$, while the latter goes through a maximum as a function of ρ at $\omega_\mu/\omega_p=0.6124$ when $\epsilon+1.666=0$. In fact, this can be directly obtained from our expression[6]

$$(\epsilon+2)/(\epsilon-1)=\pm\alpha_m\ , \tag{24}$$

with

$$\alpha_m=j_m(R_1R_2/a^2)^{3/2}=j_m\rho^{3/2}(1+\rho)^{-3}\ ,$$

with $j_m=-1$ or 2 for $m=\pm 1$ or 0 and $j_m=0$ for noninteracting particles. This shows that the resonant modes (for $k\to 0$) occur at

$$(\omega_\mu/\omega_p)^2=(1\mp\alpha_m)/3 \tag{25}$$

(Table III). Notice that the negative sign in (24) is important: two other resonances are indeed predicted to be at $\epsilon+2.428=0$ (for $m=\pm 1$) and at $\epsilon+1.4=0$ for $m=0$ leading to *absorption* peaks (ir active when $R_1\neq R_2$) at $0.54\omega_p$ and $0.6455\omega_p$, respectively. The $m=\pm 1$ peaks are degenerate and

TABLE III. Mode positions of an equal-sized—sphere binary cluster in the long-wavelength limit and the dipolar ($l=1$) approximation. Column NI refers to the noninteracting case.

$\alpha_m^2=j_m^2R_1^3R_2^3/a^6=j_m^2\rho^3/(1+\rho)^6$					
m		± 1	NI	0	
j_m		-1	0	2	
ρ	1	1		1	1
$\epsilon=\dfrac{-2\mp\alpha_m}{1\mp\alpha_m}$	-1.6666 $(-\frac{15}{9})$	-2.4286 $(-\frac{17}{7})$	-2.0	-3.0	-1.4 $(-\frac{7}{5})$
$\dfrac{\omega_\mu^2}{\omega_p^2}=\dfrac{1\mp\alpha_m}{3}$	0.375	0.29166	$\frac{1}{3}$	0.25	0.4166
ω_μ/ω_p	0.61237	0.54006	0.57735	0.5	0.6455

can be observed only when the $E_\perp$ component has a finite value. Notice also from Figs. 11 and 12 how incorrect the $k \to 0$ limit is in predicting the peak positions (except at $\rho = 1$).

It is also *extremely important* in our opinion to stress the fact that the numerical values hereby obtained are for a vacuum matrix. In a polarizable matrix (e.g., water, for which $\epsilon_M \simeq 80$), it is easy to see that the resonance modes would drastically shift toward lower frequencies and pile up at the lower end of the spectrum.

The size influence on the mode positions can be compared in Figs. 11 and 12. On the latter the constant-size particle has a 100-Å radius. The CA lines are identical to that of Fig. 11 and the symbols to the approximation of Sec. IV. Our calculated high-frequency modes tend toward the $\omega_s/\omega_p = 0.577$ value (for $\epsilon + 2 = 0$), and their variation is not as smooth as in the case $R_2 = 10$ Å, in particular at small ρ. The low-frequency modes, on the other hand, start from ω_s/ω_p, steadily merge toward the noninteracting-sphere "bulk mode" (after a plateau like region between $\rho = 1$ and $\rho \simeq 3$), and markedly decrease toward a zero value. A visual extrapolation gives the critical radius $R \simeq 4500$ Å for the recovery of the "bulk value."

The overall picture is in this case ($R_1 = 100$ Å) more sensible than in the previous one. Indeed when a "large-" (1000-Å) and a "medium-" size particle (100-Å) are in contact, one expects to recover two modes characterizing the fact that the bulk and the surface properties have to appear in the problem solution. Notice that the surface mode of the isolated 100-Å-radius sphere has some curvature as a function of ρ near $\rho = 1$.

The "critical size" for bulk properties can be also recovered by examining the variation of the mode positions as a function of one of the particle sizes when both have equal radii, i.e., $\rho = 1$ (Fig. 13). As previously noticed (Fig. 7), only three modes exist: One for the $E_{||}$ and $H_{||}$ geometries, but two for the $E_\perp$, one of them being approximately at the same frequency as that of the $H_{||}$ mode. The three characteristic modes ω_s, $\omega^{(0)}$, and $\omega^{(\pm 1)}$ obtained when a Drude dielectric constant is used are also shown on the figure. The characteristic isolated-sphere surface mode always falls between the interacting-sphere modes. However, all tend toward low-frequency values in a very similar manner. For $R \leq 10$ Å, a dashed line indicates the approximate position of the shadow-effect mode. It falls exactly in the middle of the interval spanned by the $E_{||}$ and $H_{||}$ modes. Furthermore an extrapolation at high R indicates that $\omega_\mu = 0$ near $R = 4500$ Å.

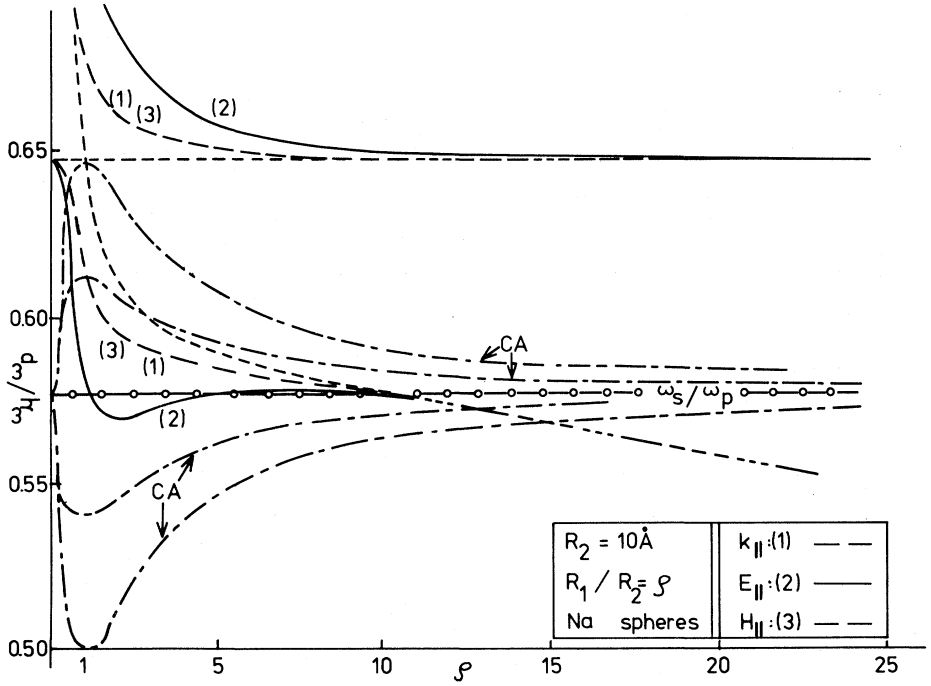

FIG. 11. Trends of the various ir resonant modes of a binary cluster of two touching and interacting sodium spheres in a vacuum matrix and for various incident polarized electromagnetic plane waves as a function of the radius ratio $\rho = R_1/R_2$. —○— line is for the noninteracting case. The CA lines correspond to the CEL theory (Ref. 13) extended in Ref. 15 with a Drude dielectric constant, but with $R_1 \neq R_2$, or to our $k = 0$ limit (Sec. IV). One of the spheres has always a radius $R_2 = 10$ Å.

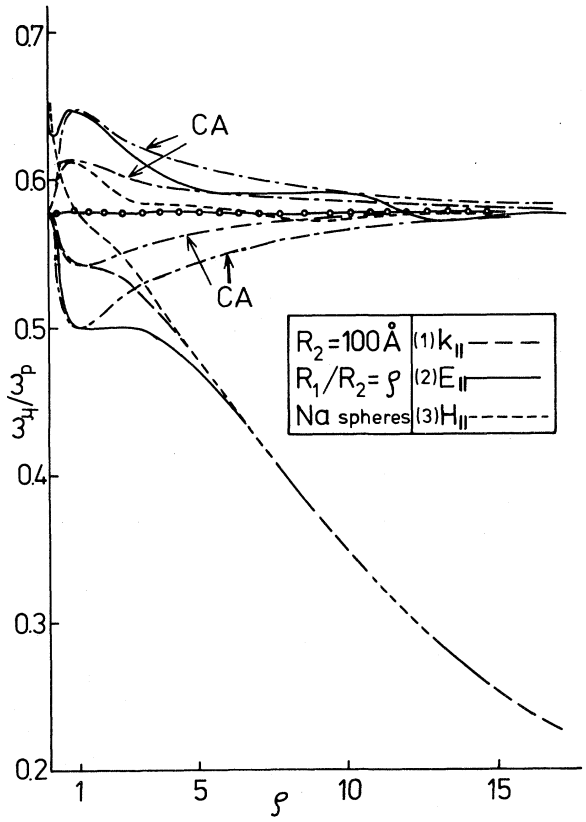

FIG. 12. Same as Fig. 11 but when the radius of the constant size sphere is $R_2 = 100$ Å.

This value is very reasonable as it characterizes bulky spheres and gives further confidence for the theory. Indeed it has the order of magnitude of the characteristic irradiation wavelength above which an assumption of constant electric polarization field in the particles (hence the neglect of high-order polar fluctuations) becomes unrealistic. Notice that the characteristic plasmon wavelength in bulk Na is about 2179 Å while that of the surface plasmon is 3770 Å. However, this also shows that the notion of "bulk" depends on the experimental investigation process.

Even though we cannot directly compare to experimental results, we expect our theory to be useful in connection with the more controllable techniques of particle distribution (like the "jet technique"[30]) and the wave-guide transmission measurements.[31]

A final warning is in order: We do not want to mislead the reader on the definite values of the particular frequencies predicted here. We stress again that they are obtained in a dipolar approximation. It is most likely that several of the quantitative conclusions will be only weakly changed when other geometries, other clusters, etc., are considered. Nevertheless, there is no doubt for us that the inclusion of higher polar-interaction terms will quantitatively change the peak positions. We briefly present in Appendix A a quantitative evaluation of such effects when the dielectric constant has a very simple form, and the long-wavelength—limit approximation is used.

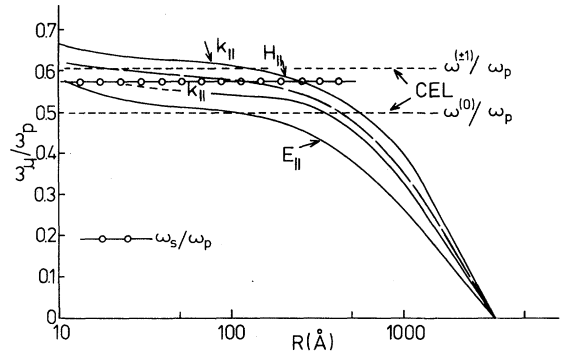

FIG. 13. Trends of the various ir resonant modes ω_μ of a binary cluster of two touching equal-sized sodium spheres of radius R in a vacuum matrix, and for various incident polarized electromagnetic plane waves as a function of R on a log scale. Noninteracting-sphere case is shown by a discontinuous line. Shadow effect precludes the observation of one peak in the $k_{||}$ geometry below $R = 15$ Å as indicated by the dashed line.

APPENDIX A

In this appendix, we use the $k \to 0$ limit of our general theory in order to estimate the qualitative and quantitative changes on the mode positions, and hence on the spectra of metallic spheres interacting not only through the dipolar fluctuations but also through higher-order polar fluctuations (viz., here the quadrupolar and octupolar modes). Such changes are of course the greatest when the spheres are in contact. We thus let $a = R_1 + R_2$. Notice that in Ref. 3 we had already shown the effect of quadrupolar-order interactions on two MgO spheres in contact, and the effect of quadrupolar- and octupolar-order interactions on the tetrahedron and on a planar five-sphere cluster in Refs. 7 and 4, respectively (long before the appearance of Ref. 16). Owing to the difference in the dielectric functions the exact mode positions and the associated absorption spectra are slightly different in the case of dielectric and metallic spheres. However, the mode positions are all implicit solutions of the relation

$$\epsilon = -(l+1)\epsilon_M F(\rho)/l \ , \tag{A1}$$

where $F(0) = F(\infty) = 1$, in either case.[6]

For future reference we will call ω_Q and ω_O the solution of (A1) when $\rho \to \infty$ or 0 and $l = 2$ and $= 3$,

TABLE IV. Infrared-active—mode positions of the equal-sized—sphere binary cluster in the long-wavelength limit in the dipolar ($D,l=1$), quadrupolar ($Q;l=2$), and octupolar ($O;l=3$) approximations). Asymptotic values for $\rho\to\infty$ are given in the last column. The modes underlined by a continuous (dashed) line are infrared absorbing when the light incidence is parallel (perpendicular) to the symmetry axis passing through the sphere centers.

	$\omega_{lm}/\omega_p\times10^4$			
	$\rho=1$			$\rho=\infty$
$\lvert m\rvert$	$l=1$	$l=2$	$l=3$	
0			7674	
1			7259	
2			6734	
3			6602	$\omega_O/\omega_p\int_{(l=3)}=0.654\,65$
3			6490	
2			6438	
1			6478	
0			6535	
0		7213	6408	
1		6834	6419	
2		6434	6437	$\omega_O/\omega_p=0.632\,46$ $_{(l=2)}$
2		6213	6161	
1		6082	5977	
0		6094	6093	
0	6455	6046	5891	
1	6124	5983	5957	$\omega_D/\omega_p=0.577\,35$ $_{(l=1)}$
1	5401	5213	5034	
0	5000	4576	4229	

respectively. The corresponding Fröhlich mode (ω_s) will be relabeled ω_D. Thus,

$$\bar{\omega}_\mu^2=\omega_\mu^2/\omega_p^2=[1+(l+1)\epsilon_M/l]^{-1}\,, \tag{A2}$$

when $\rho=\infty;\mu\equiv D,Q,O$.

The total number of nondegenerate resonant modes for N spheres (in contact and forming a linear chain) is easily found from the size S of the interaction matrix for a given m, i.e., $S=Nl,Nl,N(l-1),N(l-2),\ldots,$ for $m=0,1,2,3,\ldots$. A simple summation of the various S implies that such a number is $Nl(l+3)/2$. The number of active modes (i.e., all those for $m=0,\pm1$) is $2Nl$. This shows that there are, respectively, four, six and eight modes collapsing on ω_D, ω_Q, and ω_O when $\rho\to\infty$. The mode values at $\rho=1$ and ∞ are given in Table IV, while their position variation as a function of $\rho=R_1/R_2$ is given in Figs. 14 and 15. (Notice that such results do not depend on the exact sizes of the particles due to the $k\to0$ limit.) The

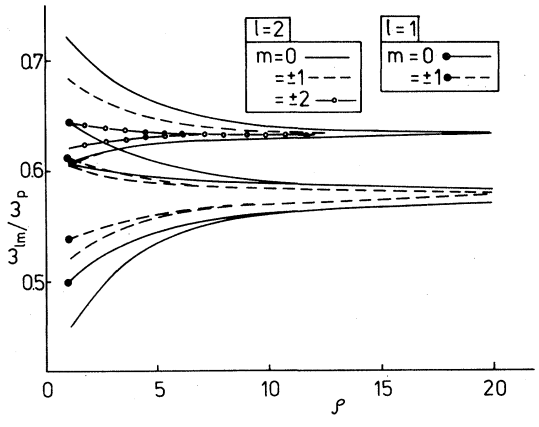

FIG. 14. ir absorption modes of a binary cluster of two *touching* interacting spheres in vacuum in the dipolar ($l=1$) and quadrupolar ($l=2$) approximations for the various polarizations (m) as a function of the sphere radius ρ in the long-wavelength limit.

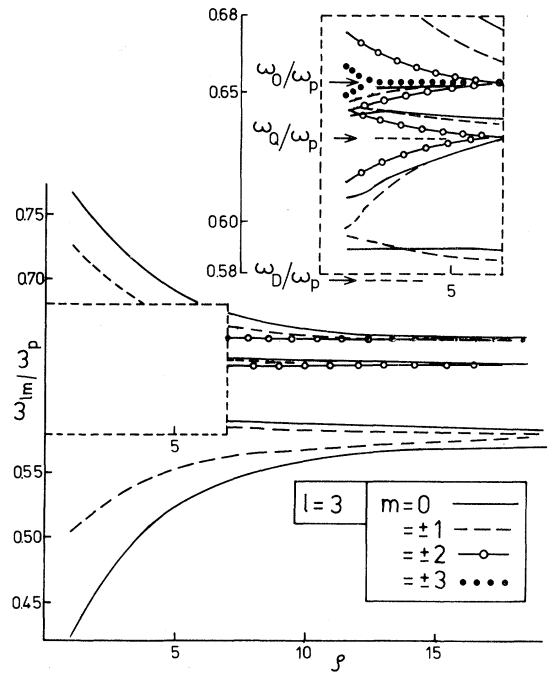

FIG. 15. ir absorption modes of a binary cluster of two *touching* interacting spheres in vacuum in the octupolar approximation ($l=3$) in the long-wavelength limit and for various polarization modes ($m=0,\pm1,\pm2,\pm3$) as a function of the sphere radius ratio ρ. Inset shows the $\rho\simeq1$ vicinity.

spectra are not displayed here. The order of magnitude of the main peaks does not vary much. It can be noticed from Table IV (or from the spectra) that an accumulation of peaks occurs between 0.60 and 0.64. Such an accumulation would be further reinforced when l increases. On the other hand, the lower-frequency and upper-frequency resonant modes (which are $m=0$ modes) continuously (and rapidly) move away from the spectrum's central region.

Such an analysis thus reinforces two main conclusions of Sec. V. On one hand, the peak accumulation in the central region might be seriously misleading those attempting to identify the $m=0$ most important mode near $\omega/\omega_p\simeq0.6$. Indeed the position of the *maximum* in the absorption spectrum might not be at the value of the dipolar mode, since such a maximum rather represents a combination of absorption amplitudes due to binary clusters (or more generally to pairs of particles), oriented more or less randomly in the matrix. In so doing one might again wonder about conclusions drawn for so-called "single-particle" properties, like the absorption spectrum, and request a new analysis of experimental data as those reviewed in Ref. 28. Notice the broadness of the spectrum (sometimes as large as 200 nm) and the double-peak structure observed for the largest ($R>40$ Å) particles obviously similar to those shown on the preceding figures.

Secondly, attempts to deduce single-particle properties from dipolar approximation formulas are likely incorrect when the spectral bounds are used as inputs, in particular if the particle density is not low nor the distribution homogeneous.

The mode-position variation as a function of ρ also shows how important the knowledge of the particle-size distribution may be with respect to data analysis pertaining to "isolated" (or single) particles.

APPENDIX B

In this appendix we explicitly define the $\vec{k},\vec{E}_0,\vec{H}_0$ vectors of the incident magnetic wave upon a cluster centered at the origin of a reference frame (x,y,z) characterized by unit vectors $\vec{1}_x,\vec{1}_y,\vec{1}_z$. Three Euler angles define the $\vec{k},\vec{E}_0,\vec{H}_0$ system, i.e., α,β,γ. The angles α and γ have been defined in Sec. II and in Fig. 2. They are, respectively, the angle between the $\vec{k}$ and the $\vec{1}_z$ vector and the polarization angle of the electromagnetic wave. The angle β is the usual longitudinal angle, between the projection of the $\vec{k}$ vector on the (x,y) plane and the x axis. Such an angle is irrelevant in the case of a binary cluster due to the cylindrical symmetry (around the z axis). It can be thus taken equal to zero, thereby assuming that the $\vec{k}$ vector is always in the (x,z) plane. Nevertheless the following formulas are written in terms of β as well:

$$\vec{k}=|\vec{k}|(-\sin\alpha\cos\beta\vec{1}_x+\sin\alpha\sin\beta\vec{1}_y+\cos\alpha\vec{1}_z),$$

$$\vec{E}_0=|\vec{E}_0|[(\cos\alpha\cos\beta\cos\gamma-\sin\beta\sin\gamma)\vec{1}_x-(\cos\alpha\sin\beta\cos\gamma+\cos\beta\sin\gamma)\vec{1}_y+\sin\alpha\cos\gamma\vec{1}_z],$$

$$\vec{H}_0=|\vec{H}_0|[(\cos\alpha\cos\beta\sin\gamma+\sin\beta\cos\gamma)\vec{1}_x-(\cos\alpha\sin\beta\sin\gamma-\cos\beta\cos\gamma)\vec{1}_y+\sin\alpha\sin\gamma\vec{1}_z].$$

[1]The basic reference is *Electrical Transport and Optical Properties of Inhomogeneous Media,* (Ohio State University, 1977), Proceedings of the First Conference on the Electrical Transport and Optical Properties of Inhomogeneous Media, edited by J. C. Garland and D. B. Tanner (AIP, New York, 1978).
[2]J. M. Gérardy and M. Ausloos, Phys. Rev. B 26, 4703 (1982).
[3]J. M. Gérardy and M. Ausloos, Phys. Rev. B 22, 4950 (1980).
[4]J. M. Gérardy and M. Ausloos, Surf. Sci. 106, 319 (1981).
[5]M. Ausloos, P. Clippe, and J. M. Gérardy, Le Vide Les Couches Minces, Suppl. 21, 758 (1980).
[6]J. M. Gérardy and M. Ausloos, Phys. Rev. B 25, 4204 (1982).
[7]J. M. Gérardy and M. Ausloos, in *Recent Developments in Condensed Matter Physics,* edited by J. T. Devreese, L. Lemmens, V. Van Doren, and J. Van Royen (Plenum, New York, 1981), Vol. 3, p. 347.
[8]G. Mie, Ann. Phys. (Leipzig) 25, 377 (1908).
[9]R. Clanget, Optik (Stuttgart) 35, 180 (1982).
[10]E. Simanek, Phys. Rev. Lett. 38, 1161 (1977).
[11]E. Simanek, Solid State Commun. 31, 419 (1979).
[12]R. Ruppin, Phys. Rev. B 11, 2871 (1975).
[13]P. Clippe, R. Evrard, and A. A. Lucas, Phys. Rev. B 14, 1715 (1976).
[14]M. Ausloos, P. Clippe, and A. A. Lucas, Phys. Rev. B 18, 7176 (1978).
[15]P. Clippe and M. Ausloos, Phys. Status Solidi B 110, 211 (1982).
[16]R. Ruppin, Phys. Rev. B 26, 3440 (1982).
[17]F. Claro (unpublished).
[18]C. G. Granqvist, N. Calander, and O. Hunderi, Solid State Commun. 31, 249 (1979), and references therein.
[19]J. M. Gérardy and M. Ausloos (unpublished).
[20]A. A. Lucas, A. Ronveaux, M. Schmeits, and F. Delanaye, Phys. Rev. B 2, 5372 (1975).
[21]R. W. Rendell, D. J. Scalapino, and B. Muhlschlegel, Phys. Rev. Lett. 41, 1746 (1978).
[22]M. Abramowitz and I. A. Stegun, *Handbook of Mathematical Functions* (Dover, New York, 1972).
[23]A. R. Melnyk and W. Harrison, Phys. Rev. B 2, 835 (1970).
[24]B. Jeffreys, Geophys. J. R. Astron. Soc. Can. 10, 141 (1965).
[25]M. A. Smithard and M. Q. Tran, Helv. Phys. Acta 46, 869 (1974).
[26]M. A. Smithard, Solid State Commun. 14, 407 (1974).
[27]L. Genzel, T. P. Martin, and U. Kreibig, Z. Phys. B 21, 339 (1975).
[28]J. A. A. J. Perenboom, P. Wyder, and F. Meier, Phys. Rep. 78, 173 (1981).
[29]We also realize that the $R \rightarrow 0$ limit has to be taken with caution in a classical calculation like here, but particles with a radius less than 10 Å do not seem to appear in the literature.
[30]W. D. Knight, Surf. Sci. 106, 172 (1981).
[31]J. E. Sansonetti and J. K. Furdyna, J. Appl. Phys. 50, 2899 (1979).